IEEE TRANSACTIONS ON INDUSTRIAL ELECTRONICS, Volume 71, Issue 3, March 2024, pp. 3163-3172
DOI:10.1109/TIE.2023.3265034

A Fiber-guided Motorised Rotation Laser Scanning Thermography Technique for Impact Damage Crack Inspection in Composites

Haochen Liu, *Member, IEEE*, Lawrence Tinsley, Kailun Deng, Yizhong Wang, Andrew Starr, Zhenmao Chen and Yifan Zhao, *Senior Member, IEEE*

***Abstract*— Laser Thermography manifests superior sensitivity and compatibility to detect cracks and small subsurface defects. However, the existing related systems have limitations on either inspection efficiency or unknown directional cracks due to the utilization of stationary heat sources. This article reports a Fiber-guided Motorised Rotation Laser-line Scanning Thermography (FMRLST) system aiming to rapidly inspect cracks of impact damage with unknown direction in composite laminates. An optical head with fibre delivery integrated with a rotation motor is designed and developed to generate novel scanning heating in a circumferential rotation manner. A FEM model is first proposed to simulate the principle of FMRLST testing and produce thermograms for the development of post-processing methods. A damage enhancement method based on Curvelet Transform is developed to enhance the visualization of thermal features of cracks, and purify the resulting image by suppressing the laser-line heating pattern and cancelling noise. The validation on three composite specimens with different levels of impact damage suggests the developed FMRLST system can extract unknown impact surface cracks efficiently. The remarkable sensitivity and flexibility of FMRLST to arbitrary cracks, along with the miniaturized probe-like inspection unit, present its potential in on-site thermographic inspection, and its design is promising to push the LST towards.**

***Index Terms*— Motorised Rotating Laser-line; Laser scanning thermography; Barely Visible Impact Crack (BVIC); Curvelet Transformation; Composite laminates.**

Manuscript received xx, 2xxx; revised xx, xxxx; accepted xx, xxxx. This work was supported by the UK EPSRC Platform Grant: Through-life performance: From science to instrumentation (Grant number EP/P027121/1).

Haochen Liu, Lawrence Tinsley, Yifan Zhao, Yizhong Wang, Kailun Deng and Andrew Starr are with the School of Aerospace, Transport and Manufacturing, Cranfield University, Cranfield, MK43 0AL, UK. (e-mail: haochen.liu@cranfield.ac.uk; l.tinsley@cranfield.ac.uk; yizhong.wang@cranfield.ac.uk; kailun.deng@cranfield.ac.uk a.starr@cranfield.ac.uk; corresponding author: yifan.zhao@cranfield.ac.uk).

Zhenmao Chen is with State Key Laboratory for Strength and Vibration of Mechanical Structures, School of Aerospace, Xi'an Jiaotong University, Xi'an, 710049, China (e-mail: chenzm@mail.xjtu.edu.cn).

I. Introduction

COMPOSITES play an increasingly dominant role in material science, technology innovation and advanced structures. Modern aviation and transportation structures manufacturers pay more attention to multiple types of composite laminates including Carbon Fiber-reinforced Polymer (CFRP), Glass Fiber-reinforced Polymer (GFRP) and nanocomposites as dominant material for high-strength skeletons, heavy-loading parts and complex enhanced structure. Due to their advantages of low density, high structural strength, adjustable mechanical properties and high resistance to corrosion and abrasion, composites are quickly expanding their usage and applications in aerospace, space, automotive, nuclear, civil and renewable energy industries [1-3]. However, the integrity and mechanical stability of advanced composites are threatened by damage and degradation caused by low-velocity impact, maintenance tools or ground vehicle strikes, long period overloading and severe or varying service environment. Ostensibly, damage profiles such as cracks in Barely Visible Impact Damage (BVID) are relatively small and seem to be harmless, i.e. falling within the allowed damage size according to the aircraft's structural repair manual. But internal structural damage could be fatal and penetrating through the material may result in catastrophic failures [4].

The inspection of surface cracks caused by impact energy is of great importance to ensure the safety and operation of composite laminates. Non-destructive Testing and Evaluation (NDT&E) has been proven to be an effective & reliable tool to detect, assess and monitor multiple damages including cracks [5, 6]. For cracks in different materials (either metallic or composites), several typical methods, including Visual Testing (VT), Eddy Current Testing (ECT), Ultrasonic testing (UT), Radiographic Testing (RT), etc. are well studied in both crack inspection and quantification [7-10]. However, they are incapable of either non-contact remote inspection, fast inspection for a large area or subsurface detection. InfraRed Thermography (IRT) is a powerful NDT technique that offers rapid, non-contact, robust non-invasive inspection and real-time monitoring. With many practical applications for

ceramics, plastics, composites and coatings [11-13], it has presented advantages in material suitability, inspection efficiency and cost budget compared to other NDT techniques. Among multiple variants of active IRT with different heat sources, Laser Thermography (LT) manifests superior sensitivity and compatibility to crack and small subsurface defects due to its concentrating heating and thermal expanding mechanism [14]. The original form of Laser Spot Thermography (LST) [15] was first designed to focus cracks in metallic and then introduced to composites. But the inspection efficiency of LST is mediocre, and the quantification is challenging as the beam spot is normally too small to cover an entire crack.

To improve LST, Laser-Line Scanning Thermography (LLST) was a prominent step forward in inspection efficiency, where a laser-line beam is actuated with an orthogonal scanning direction to laser-line, sweeping across the inspected area [16]. The scanned crack edges are sensitively responding to the dynamic thermal pattern that is triggered not only by a thin-long line beam but also a scanning heat inducement area, therefore generating a clear thermal contrast in an inspection. However, the 1-dimensional concentrated laser-line of LLST reduces its inspection superiority to cracks that are orthogonal to the line due to its 1-dimensional thermal transfer mechanism. LLST is widely recognized as not fully capable of all unknown directional cracks when inspecting complex surface cracks in composites with only single scanning. Another promising alternative, Laser Array Spot Thermography (LAST) [17], was designed to project the laser beam in the form of an array to cover a large area to increase inspection efficiency. The shaped array spot beams inherit the advantage of full-directional thermal transfer from LST. Therefore, it is more compatible than LLST for cracks with unknown directions [18]. But as a stationary heat source, it is still not as fast as LLST to implement full coverage of a large area. Additionally, its optical head is more complicated and costly.

To expand the applicability and versatility, the fiber-guided LST is a solid enhancement in the accessibility and miniaturization [19] of the system for applications with confined space. The soft laser fiber fused with a customized optical head can transude almost all laser energy through a flexural path, enabling the possibility of a probe-like heat source that leaves the bulky laser generator away [20]. Several studies have reported the feasibility of the fiber-guided LST in the applications for the inspection of coating thickness and laminates dis-bond using laser spot, line scanning thermography and LAST. These studies prove that fiber-guided heating is a valuable and safe system towards advance LT inspection [21]. However, most LST studies use the fiber-guided as a stationary heat source. The actuation and miniaturization for the scanning fiber-guided optical head for thermography scanning automation is still limited.

To improve the inspection of unknown arbitrary surface cracks in composite, a Fiber-guided Motorised Rotation Laser Scanning Thermography (FMRLST) is proposed in this paper. The novelty of FMRLST lies in below aspects:

1) The FMRLST presents superior sensitivity, flexibility and detectability for arbitrary direction cracks, providing a more versatile rotating heat transfer mechanism compared to traditional linear line-scanning.
2) The corresponding FEM simulation and image processing algorithm supports FMRLST with useful tools for pre-inspection thermal feature prediction, and post-inspection defect enhancement & extraction.
3) A probe-like optical head heat source vigorously promotes the miniaturization and accessibility of LST in in-site inspections.

This paper is organized as follows. Section II presents the methodology and the structure of FMRLST. Section III describes the FEM modelling and experiment system of FMRLST and the inspection results and discussion are presented in Section IV. Finally, the conclusions are summarised in Section V.

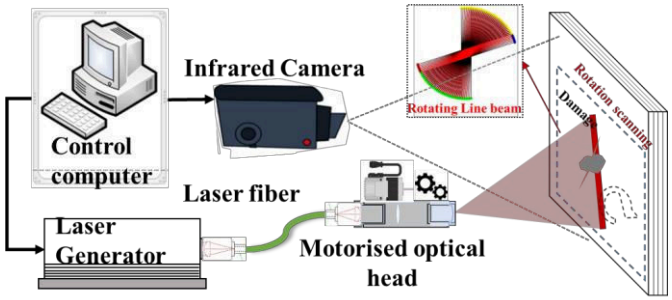

Fig. 1. Principle of the FMRSLT.

II. METHODOLOGY AND SYSTEM DESIGN

A. Fiber-guided Motorised Rotation Laser-line Scanning thermography (FMRLST)

The proposed FMRLST system is an upgraded heating manner technique based on laser scanning thermography with a principal architecture shown in Fig. 1. It consists of an optical head for scanning excitation, an infrared camera for data capturing, a corresponding control unit, and an image sequence processing method. The laser heating module is composed of a fiber-coupled laser generator, a diode laser control unit, and a motorized optical head. A Continue Wave (CW) 976nm fiber-guided diode laser is employed to provide 5W power heating in this study, achieving flexible heating pointing and a miniaturized excitation head. The sensing module is a

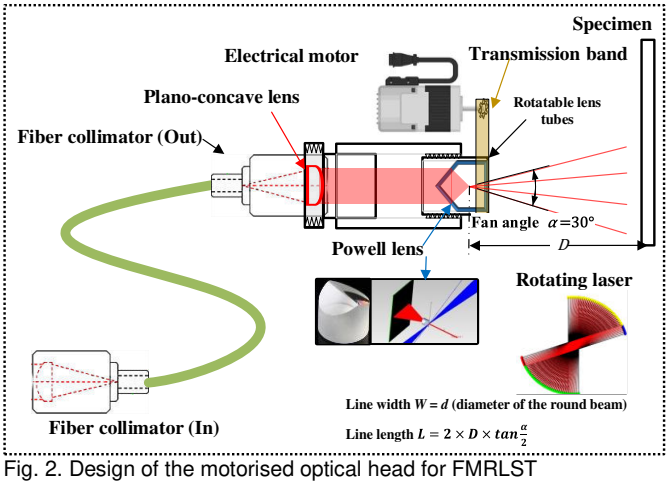

Fig. 2. Design of the motorised optical head for FMRLST

long-wave infrared camera with a wavelength of 7-14μm that is totally distinguished from the 976nm laser, avoiding the reflective optical interference from the laser excitation.

The detailed diagram system setup is shown in Fig. 2. The induced laser is first collimated into a laser fiber and guided to the output end, then collimated to be a Gaussian distributed round beam by a Plano-concave lens. The optical head consists of a lens tube and a rotatable lens mount, installing a Powell lens that reshapes the round beam to a line beam. Finally, an electrical motor is integrated to rotate the Powell lens by a power transmission band, generating a rotating line beam pattern. The width of the line beam is equal to the diameter of the round laser beam, and the length of the line beam is subject to $L = 2 \times D \times tan\frac{\alpha}{2}$, where α, D denote the Powell lens fan angle and the distance to the specimen.

The novelty of this FMRLST is that it provides a more versatile heat transfer mechanism for crack inspection, compared to traditional linear line-scanning. As most cracks are straight lines but with multiple directions, the traditional linear line-scanning is required to find the optimal laser scanning mode (laser parallel to the crack) to obtain the high defect contrast, which results in difficulty for defective specimens with unknown directions. Differently, the FMRLST creates an angular dynamic heat transfer and utilizes the tangential defect thermal feature between the laser line and cracks. This mechanism has general applicability and sensitivity to arbitrary directions of cracks and brings attractive convenience for laser thermography in an in-situ inspection.

B. FEM Simulation

In order to comprehensively investigate thermal features and conduction characters in the FMRLST inspection cracks CFRP, a numerical simulation based on FEM has been conducted as a convenient tool for the provision of flexibility and stability for signal prediction. Based on the Fourier transfer Law, the heat transfer mechanism follows the (1)

$$[\kappa]_{An}\{\nabla\}^T\{\nabla\}T - \left(\rho c_p\right)_{eff}\dot{T} = -Q|_{\Gamma(X(r,\omega,t),\,Y(r,\omega,t),\,t)} \quad (1)$$

where T and $\{\nabla\}$ denotes the gradient vector of the Cartesian coordinates, respectively. $[\kappa]_{An}$ and $\left(\rho c_p\right)_{eff}$ denotes the global anisotropy of heat conductivity and effective volumetric heat capacity of the material, respectively. As for the boundary condition according to the external rotation scanning heat, the $-Q|_{\Gamma(X(r,\omega,t),\,Y(r,\omega,t),\,t)}$ is the scanning excitation heat flux, in which $\Gamma(X(r,\omega,t),\,Y(r,\omega,t),\,t)$ determines the spatial dynamic heat area in the X and Y axis, subjecting to the laser-line radius r and scanning angular velocity ω on the surface.

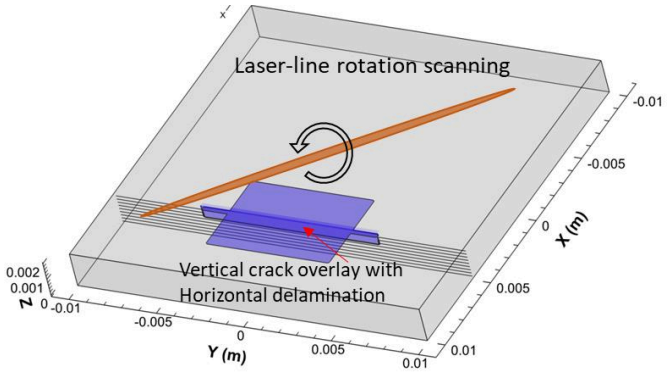

Fig. 3. FEM simulation model of FMRLST

Via representing the matrix with epoxy-resin and reinforcements by fibers acting such as pores in the heat transfer model, each ply of the model is established as a porous structure [23, 24]. Based on the above representation of the two-component system and the rule-of-mixtures, the effective heat capacity of the composite medium can be estimated from the weighted average of the specific properties of each phase based on the volume fractions:

$$\left(\rho c_p\right)_{eff} = \phi_f\left(\rho c_p\right)_f + \left(1-\phi_f\right)\left(\rho c_p\right)_m \quad (2)$$

$$\phi_f = \frac{V_f}{V_T} = \frac{V_f}{V_f+V_m} \quad (3)$$

where ϕ_f denotes the volume fractions V of the fiber. The subscripts f and m in (2) and (3) denote the fiber and epoxy-resign matrix, respectively. To account for thermal conductivity, the series-parallel model [23] is employed. The global heat conductivity can be calculated by (4)

$$[\kappa]_{An} = \begin{bmatrix} \kappa_L cos^2\theta + \kappa_T sin^2\theta & \frac{\kappa_L-\kappa_T}{2}sin2\theta & 0 \\ \frac{\kappa_L-\kappa_T}{2}sin2\theta & \kappa_L sin^2\theta + \kappa_T cos^2\theta & 0 \\ 0 & 0 & \kappa_{cp} \end{bmatrix} \quad (4)$$

where θ is the fiber orientation angle related to the X direction. The - κ_L and κ_T denotes the longitudinal and transverse equivalent thermal conductivity (i.e. longitudinal and transverse directions), and κ_{cp} = κ_T is the cross-ply conductivity. After establishing the objective model and discretization using the Galerkin FEM and meshing using the hexahedron element, the heat transfer with the model can be expressed by (5)

$$\left[[K]_{An}(1-\zeta) + \frac{\left[C_{eff}\right]}{\Delta t}\right]\{T\}_{t+\Delta t} = \{Q\}_{(X+\Delta X_t,\,Y+\Delta Y_t,\,t+\Delta t)} + \left[\frac{[\mathrm{C_{eff}}]}{\Delta t} - \zeta[K]_{An}\right]\{T\}_t \quad (5)$$

Based on the above analysis, a CFRP composite model was established, as shown in Fig. 3, where a sample was embedded with typical impact damage composed of horizontally laid delamination and a vertical crack in the Y direction representative of a transverse matrix crack. A ten-layer fiber ply model with a 45-degree angle difference in fiber orientation is established. The dimension of the CFRP model is 20 mm×20 mm×2 mm, and the thickness of each layer (ply) is 0.2 mm. The model is discretized as 400×400×40 hexahedral elements. The thermal conductivity of fiber and epoxy matrix is set as 5.00 W/(m·K) and 0.22 W/(m·K), respectively. The rotation laser-line is a Gaussian beam distribution (1/e fall) with the size of [16 mm, 1 mm] for [length, width] axis. In this model, crack and delamination are modelled with a rectangle shape, and the crack width and delamination thickness are modelled to be 100 μm. The length and depth crack is 10.0 mm and 0.3 mm, respectively. The delamination is buried at the 1st top interface, whose length and width are 7.0 mm and 6.0 mm, respectively.

C. Image processing for FMRLST

To extract the crack feature and enhance its contrast against the sound area, an image processing method is specifically designed for the FMRLST. Fig. 4 concludes the four main signal properties in thermal images from FMRLST, analyzing

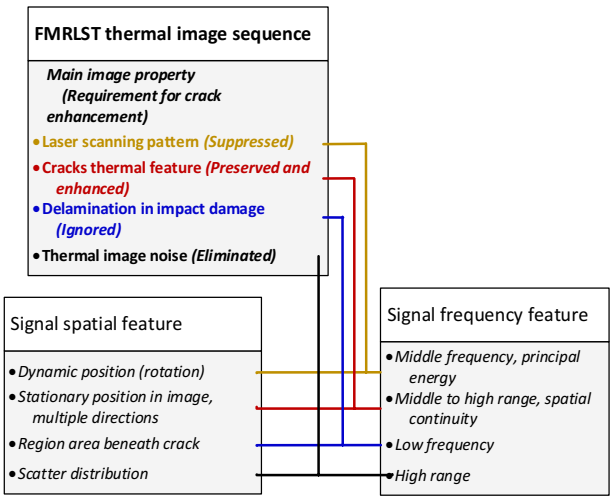

Fig. 4. Image property feature and processing requirements for crack extraction in FMRLST.

their feature in the spatial and frequency domain. Theoretically, the typical FMRLST thermal image consists of 4 main properties: laser pattern, crack feature in impact damage, delamination of impact damage and noise signals. In the spatial domain, the laser pattern (line beam) changes its direction circumferentially. And it is the only spatial dynamic signal properties compared to other stationary properties such as defects, composite surface patterns. The cracks and delamination are always overlapping due to the impact damage mechanism. The noise is under scatter distribution within the whole frame. The cracks remain linear spatial continuity rather than scatter distribution of noise.

In the frequency domain, the delamination, laser, crack and noise distribute from the low, middle to high range of frequency spectrum, respectively. In the high-frequency spectrum, there will be slight overlapping of frequency between crack and noise, but we believe the frequency of the noise feature is higher than that of the crack. At last, the laser pattern is the only dynamic feature with circumferential changes during the scan in the frequency distribution.

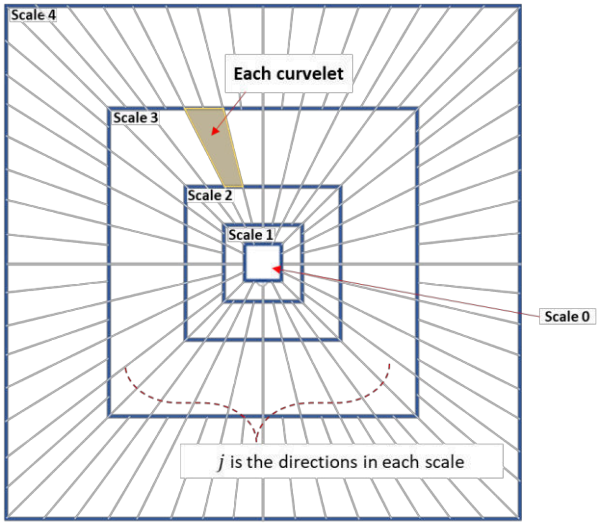

Each scale is divided into $16 \times 2^{(i-1)/2}$, i is the scale

Fig. 5. Frequency spectrum illustration of Curvelet Transform in Cartesian coordinates

Curvelet Transform (CT)

Wavelet Transform (WT) plays an important role in signal and image processing. Deriving from WT, the Curvelet Transform (CT) is designed for addressing the limitation of the WT (only catch linear feature), remedying with the more sensitivity capability for higher dimensional feature extraction (e.g. curves in images).

In CT, the image is processed in parabolic scaling with a translational and rotating manner in the frequency domain. It overcomes the limitation of curve invariance under anisotropic scaling of WT [25]. The principle of Discrete CT (DCT) for 2D images can be illustrated in Fig. 5, where curvelet elements are supported by wedges in parabolic pseudo-polar illustration in cartesian coordinates. The curvelets doubles in each second circular ring from the inner to outer scale. The definition of image CT can be expressed by (6)

$$c(i,j,\boldsymbol{k}) \coloneqq \langle f, \varphi_{i,j,\boldsymbol{k}} \rangle = \int_{R^2} f(\boldsymbol{X}) \cdot \overline{\varphi_{i,j,\boldsymbol{k}(\boldsymbol{X})}} d\boldsymbol{X} \quad (6)$$

where $\boldsymbol{X} = (x,y)^T$ represents the image pixel, $\varphi_{i,j,\boldsymbol{k}}$ is the curvelet atom at the scale i, orientation direction j and $\boldsymbol{k} = (k_1, k_2) \in \mathbb{Z}^2$ position within the curvelet. The curvelet atoms $\varphi_{i,j,\boldsymbol{k}}$ are built by the composition of a translation $\boldsymbol{X}_{\boldsymbol{k}}^{(i,j)}$ and of a rotation R_j of a mother curvelet atom φ_i as (7)

$$\varphi_{i,j,\bar{k}}(\boldsymbol{X}) = \varphi_i(R_j(\boldsymbol{X} - \boldsymbol{X}_{\boldsymbol{k}}^{(i,j)})) \quad (7)$$

where R_j is the rotation by θ_j radians. θ_j is the equi-spaced sequence of rotation angles $\theta_j = 2\pi 2^{-\lfloor i/2 \rfloor} j \in (0, 2\pi)$. The mother curvelet φ_i is defined by the mean of Fourier Transform $\hat{\varphi}_i(\boldsymbol{\omega})$ written in polar coordinates as (8)

$$\hat{\varphi}_i(r,\theta) = 2^{-\frac{3i}{4}} W(2^{-i} r) V\left(\frac{2^{\lfloor i/2 \rfloor}\theta}{2\pi}\right) \quad (8)$$

The support of $\hat{\varphi}_i$ is a polar parabolic wedge supported by W and V that is radial and angular windows, respectively (both smooth, nonnegative and real-valued). In Fig. 5, the low (inner) and high (outer) scale curvelets represent the low-frequency and high-frequency features in the image omnidirectionally. The specific curvelet in each direction represents the image

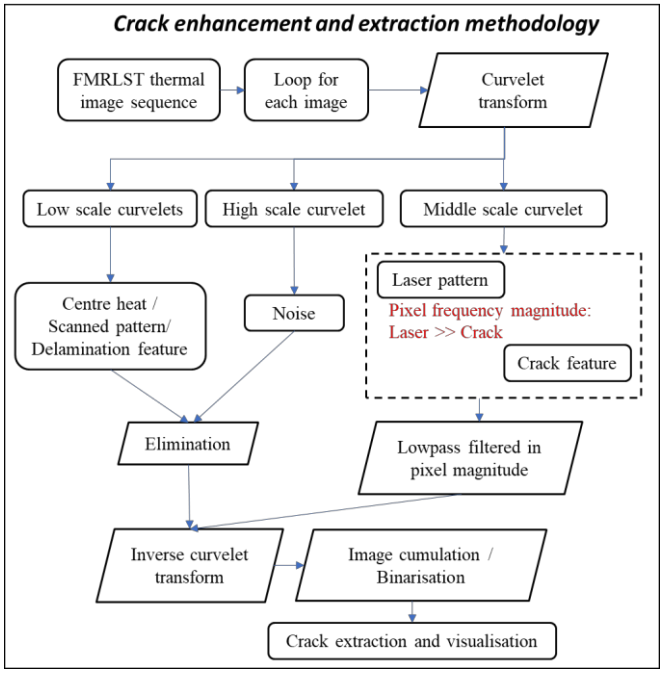

Fig. 6. Crack extraction and enhancement methodology

feature at the corresponding angle.

Therefore, according to the thermal feature of FMRLST in Fig. 4 and CT principles, the overall methodology of data processing for FMRLST can be concluded in Fig. 6. The delamination (low-frequency) has the principal presentation in the lower scales. To ignore this feature, low scales should be eliminated. The dynamic rotating laser pattern focuses on the middle scale and changes its principal distribution across different directional curvelets. And it is the strongest energy in magnitude compared to crack. To suppress the laser pattern, the high energy coefficients within each curvelet should be eliminated. Moreover, as it changes position within the sequence, it will be furtherly homogenized by an average cumulating process of the scanning sequence.

The crack feature distributes among the middle to high range in the frequency domain. More importantly, it is a spatial-stationary feature compared to the laser pattern, and spatial continuous compared to noise. Therefore, to enhance it, the middle-to-high scale should be preserved. And its contrast will be furtherly cumulated in the cumulating process. Finally, the noise is represented within the highest range scale of curvelets and distributed scattered. To mitigate the noise, these curvelet coefficients should be eliminated.

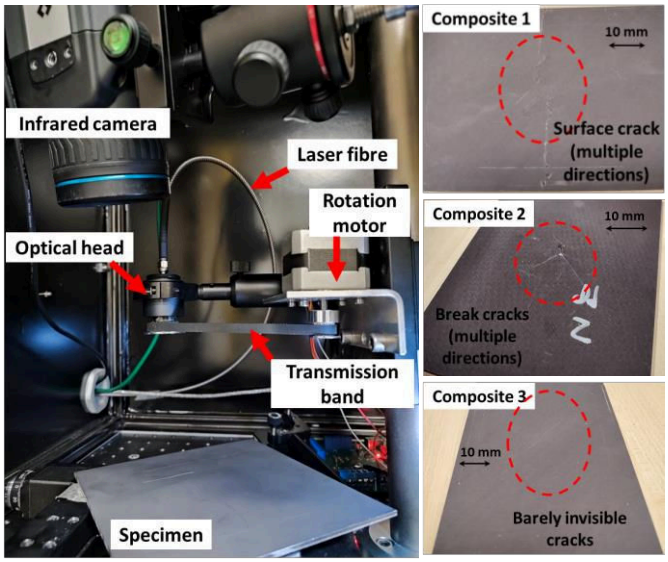

Fig. 7. FMRLST Experimental system (left) and three composite specimens with different level impact damage (right).

TABLE I
FMRLST EXPERIMENT SETUP SPECIFICATION

Items	Specification parameters
IR Camera	• IR wavelength range: 7-14 μm; • Thermal sensitivity: less than 25 mK; • Detector resolution: 640×480;
Heating source	• Continuous wave (CW) CO2 laser, 980nm; 5W power used for heating; • Laser generator beam: Gaussian beam; • The beam is shaped by line pattern Powell lens and rotating motorised; • Line beam [length, width]: [120mm, 6mm]
Rotating Laser-line scanning	• Incidence angle to samples surface: vertical; • Optical head to specimen: 160mm • Scanning angular speed: 0.35rad/s;
Data capturing	• 25 Hz sampling rate; 18 s to scan a full circle; • 500 images captured for each experiment;
CFRP Samples	• Size: 150 mm × 70 mm × 4 mm

III. EXPERIMENTAL SYSTEM

An experimental system, illustrated in Fig. 7, was designed and implemented in this study to validate the FMRLST. A laser head was established for the inspection of impact damage in the CFRP samples shown in Fig 7. The thermal images were captured by a FLIR-A615 series long-wave (7-14μm) IR camera. Table 2 gives the key technical specifications of the camera and the laser excitation source associated with the detailed experimental parameters. Between each experiment, a 10-minute interval was applied to cool the specimen.

Three defective composite laminate samples with impact damage (rear surface shown in Fig. 7) were tested using the proposed FMRLST. The Composite 1 sample has clear surface-break damage with multiple directional cracks, which is part of surface-break damage through the whole panel. The Composite 2 sample has the biggest damage with a clear bump and multiple directional surface-break cracks. The Composite 3 sample has barely visible damage, with only two small cracks.

IV. RESULTS AND DISCUSSION

A. Simulation results

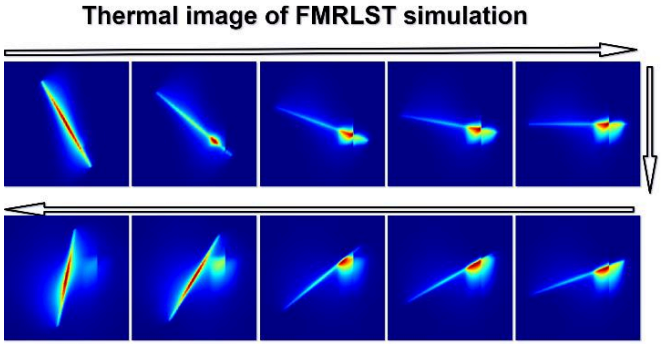

Fig. 8 Raw thermal sequence of FMRLST simulation model

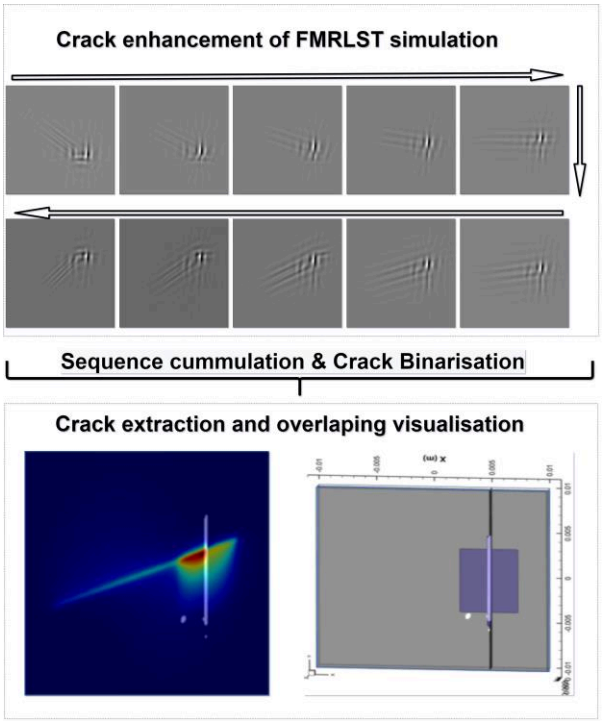

Fig. 9 Crack enhancement and extraction of simulation model.

In this section, the thermal response of the simulation model shown in Fig. 3 is presented and discussed with the experimental results. Fig. 8 presents the temperature distribution of half circle of scanning when the laser-line scans across the defect area. The thermal images of the top surface show an obvious temperature contrast on the delamination area and a dramatic discontinuity at the crack edge. And the rotating laser line can only highlight the crack partially when scans across the defect. In addition, the simulation results also show the heat transfer and defect features, e.g. a heat concentration in the rotation center, low-frequency delamination, a spatially dynamic middle-frequency feature of the laser-line, and a high-frequency feature of the crack. These prove the image analysis for the processing method and show an ideal condition image feature of FMRLST.

Furtherly, the crack extraction methodology was applied to the simulation model. The upper part of Fig. 9 lists the crack-enhanced image sequence of the CT-based image processing, which remains only a part of the crack feature in each image. After the cumulation and binarisation, the ripple effect of the crack feature was well suppressed, and the crack (white highlighted) can be clearly extracted in the low part of Fig. 9 (e.g. crack extraction and overlapping with the raw thermal image of the model). The simulation demonstrates the feasibility of the proposed method and sets a solid foundation for applicability testing on real impact damage samples.

B. Experimental results

Fig. 10. shows the raw thermal images from FMRLST scanning on the Composite 1 sample. The image time sequence follows the clockwise arrow. The laser line starts in the diagonal direction and rotates a full circle anticlockwise. In different circumferential images, cracks with multiple directions are chronologically stimulated to present high contrast with temperature rise. However, it is clear that the laser-line heating pattern occupies the dominating feature in each image that suppresses the defect contrast. As the center of the rotation scanning is heated all the time, the center temperature kurtosis is also a shortage for crack inspection.

To enhance the crack contrast, a five-scale CT-based decomposition method is applied. A raw thermal image is

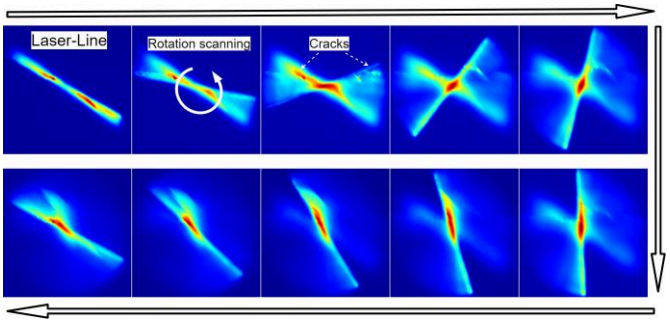

Fig. 10 Raw thermal sequence of FMRLST on the Composite 1

decomposed by CT to present the curvelet frequency spectrum image (2nd in Fig. 11). In this figure, the center is the Scale 1 curvelet which manifests the low range frequency feature representing the principal heat energy properties of the scanned area. It is clear that this scale contains the heat kurtosis of the center of rotation, residual heat after scanning and delamination of the impact damage. This Scale 1 should be eliminated for crack enhancement. The Scale 2 represents the middle-range frequency that mainly contains the laser-line feature of the current frame. The similar direction of curvelets contains the strongest laser-line feature. Scale 2 should also be eliminated for crack enhancement. It should be noted that some crack contrast is observable in the specific Scale 2 curvelets due to the slight frequency overlapping between the laser-line thermal feature and the crack feature. The elimination might cause a slight loss of the crack feature. But because the resolution of Scale 2 curvelets is still not high enough to present the crack detail texture, we believe that the main crack frequency range is still higher than the laser line. Therefore, we set zero magnitudes to all Scale 2 curvelets coefficients.

In Scale 3, the laser-line feature is clearly reduced compared to Scale 2, and the crack property is appearing with the highest intensity between curvelets. This proves that the abovementioned analysis of separated frequency ranges between the crack-related feature and the laser-line feature, even though a slight overlapping exists. Furtherly, it can be observed that the crack pixels present a higher magnitude than laser-line pixels, which provides a good chance to furtherly suppress the laser-line within Scale 3 by the cut-off of

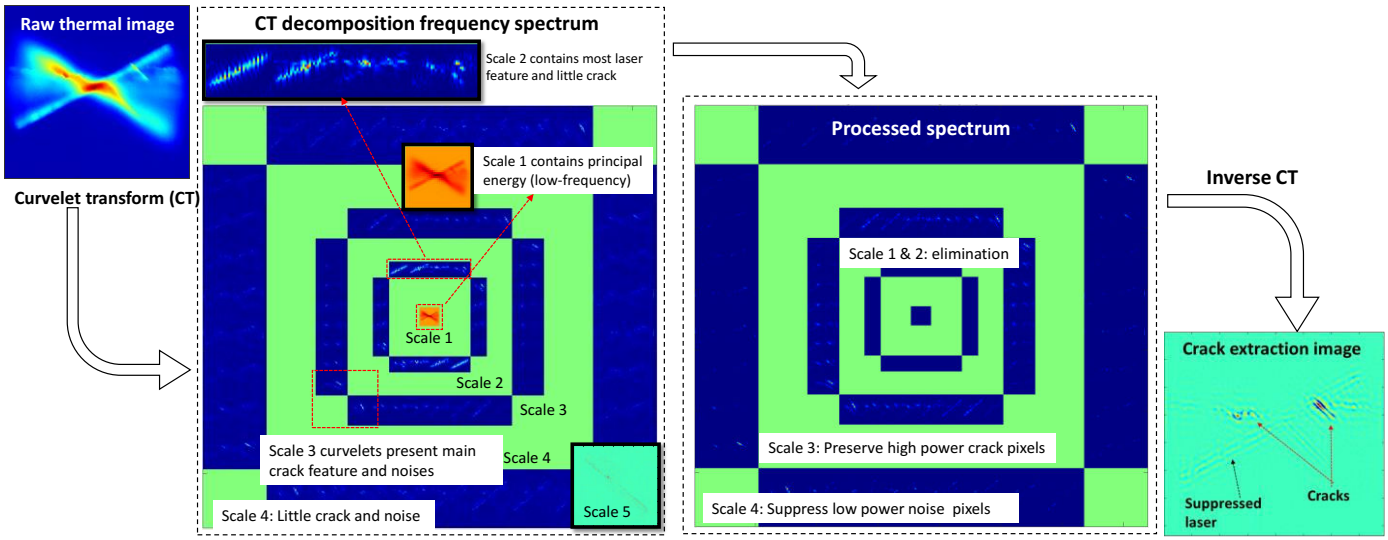

Fig. 11. Enhancement process of the curvelet spectrum for FMRLST thermal image.

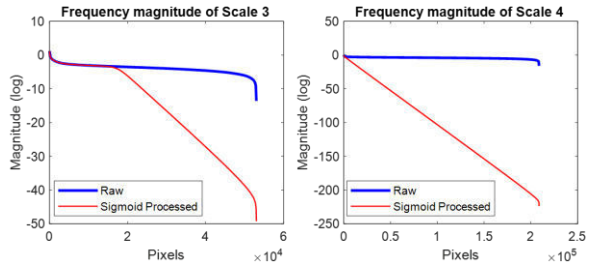

Fig. 12. The truncation of 3 and 4 Scales of curvelets pixels for crack enhancement.

frequency magnitude. In summary, to enhance the crack, Scale 3 should be preserved, and the low-magnitude pixels should be suppressed. In Scale 4, it can be observed that cracks and noises are included and distributed from high to low frequency. Therefore, the same strategy with Scale 3 is adopted for Scale 4 curvelets to cancel noise and preserve cracks. Finally, a zero setting of magnitude is also applied for Scale 5 curvelet coefficients which contain noises.

Based on the above analysis, the crack feature enhancement process of all five scales of curvelets is shown in Fig. 12. The pixels in Scale 1, Scale 2 and Scale 5 were eliminated. A truncation suppress filter was adopted for Scales 3 and 4. To avoid the ripple effect after direct truncating, the sigmoid method is also applied to smooth the truncation (see Fig.12).

Then by looping the same process to all images in the sequence, the crack enhancement of FMRLST is presented in Fig. 13. Each part in each crack is gradually highlighted by enhanced contrast along the scanning sequence. Until the laser line finishes a full circle, all cracks in multi-direction are presented. In the whole sequence, it can be observed that the laser-line feature is well suppressed for those images when the laser is scanning on cracks (e.g. 1st, 2nd and last row in Fig. 13.). When the laser is not scanning on the crack, there is a slight ripple effect of laser-line remaining in the enhanced image, such as the last two in the 3rd row. This is because, in these images, the past-scanned cracks have become blurry and caused stronger frequency overlapping between the laser line and cracks.

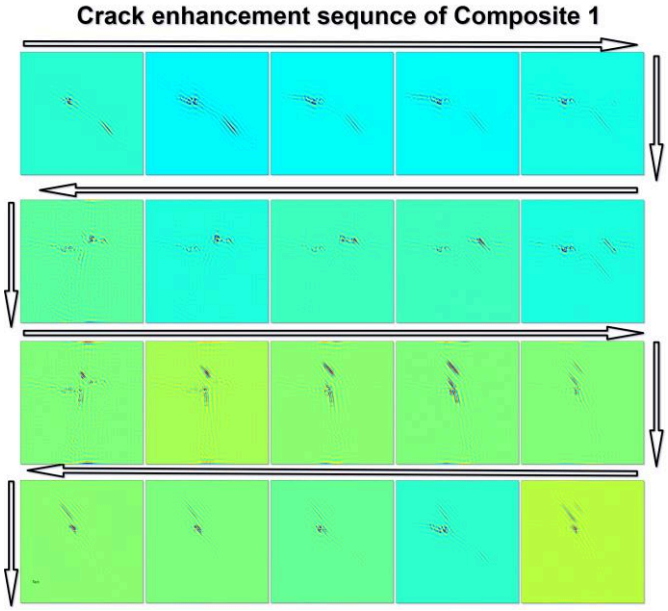

Fig. 13. The crack enhanced sequence after inverse CT.

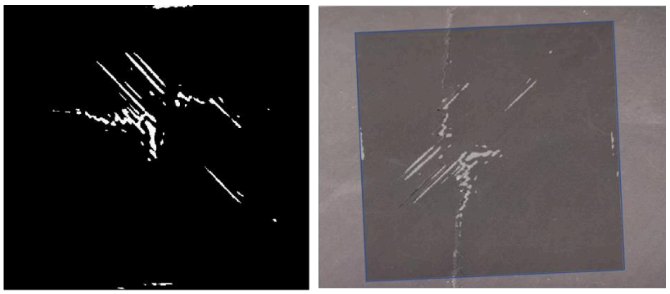

(a) (b)

Fig. 14. The extraction of the surface crack in Composite 1 specimen. (a) Binarisation image; (b) Overlapping with specimen photo.

To better extract the crack inspection results, the cumulation of the defect sequence is applied to assemble the fragmentarily enhanced feature for each crack, and furtherly suppress the laser-line influence. Then a binarization is adopted to extract them. Fig. 14 shows the final results of cumulation and binarisation. All directions cracks of Composite 1 are effectively extracted. By overlaying with the sample photos, the extracted crack image accurately fits the photo. It demonstrates the feasibility and superior effectiveness of the proposed FMRLST and associated post-processing method for multiple crack inspection in composites impact damage.

Fig. 15 and Fig. 16 present the crack enhancement and extraction results of Composite 2 and Composite 3 specimens, respectively. In Fig. 15, the surface break damage is clearly detected, including the break bump and several cracks along the surface layer fiber. Only one fiber-vertical crack is failed to be extracted. This miss inspection is caused by uncover scanning, which the crack locates outside the edge of the rotating scanning circle. In Fig. 16, the cracks in the barely invisible impact damage in Composite 3 are clearly visualized. Both the crack position and length were accurately extracted. The results of Composite 2 and 3 demonstrate the versatility of FMRLST for crack inspection in different level of composite impact damage.

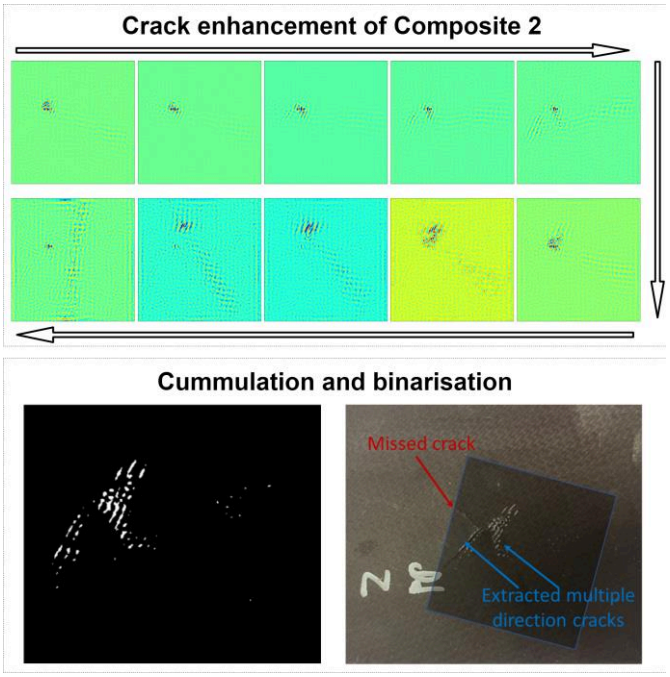

Fig. 15. The enhancement and extraction of the crack in Composite 2 specimen.

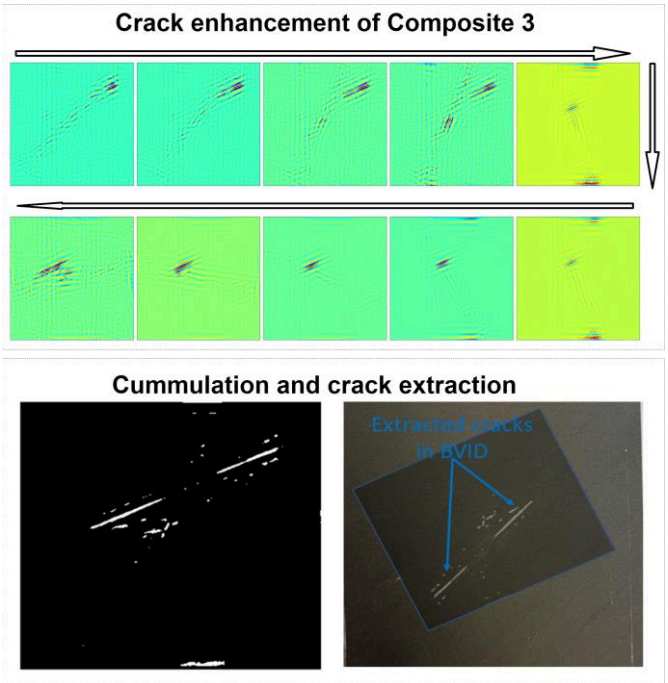

Fig. 16. The extracted cracks from BVID in Composite 3 specimen.

V. Discussion

The FMRLST shows strong sensitivity to cracks with arbitrary directions, and presents a superior spatial resolution to distinguish adjacent cracks. To compare with traditional Pulsed Thermography (PT) inspection, shown in Fig. 17, a raw image from the PT inspection and corresponding results of the 2nd-order Principal Component Thermography are compared with the results of the proposed technique. Even though the PT can detect the cracks along the first layer fiber, the cracks with other direction show poor contrast and blurry edges. In addition, it cannot distinguish two close parallel cracks which are clearly extracted by the proposed FMRLST.

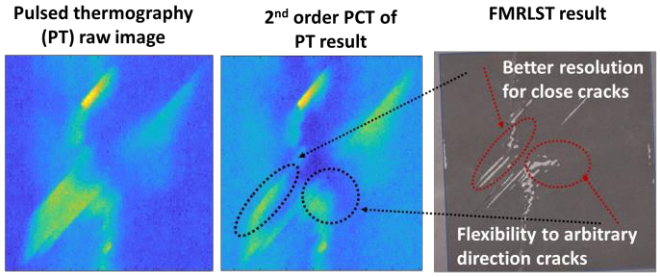

Fig. 17. Comparison to traditional pulsed thermography inspection.

In the traditional linear laser-line scanning thermography for crack inspection, it is well-known that the optimum direction of inspected crack is the one parallel to the scanning line, and the worst is the one orthogonal with the scanning line. To examine the FMRLST direction flexibility, the scanned cracks with 90° and 45° deviation to the laser-line are analyzed as examples in Fig. 18. In Fig. 18 (a) and (b), both 90°and 45° cracks are clearly excited and presents obvious anomalies of thermal features between the crack sides. In addition, being grateful to the polar coordinate-like heat transfer mechanism, the FMRLST can keep exciting clear thermal feature for the

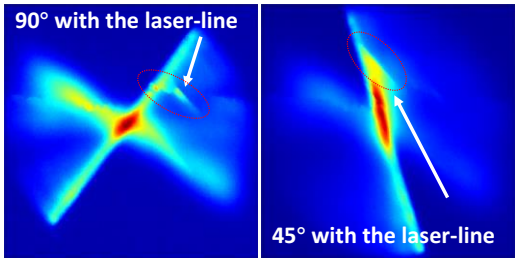

(a) (b)

Fig. 18. Flexibility to crack direction. (a) 90° to the laser line; (b) 45° to the laser line.

scanned part of crack for a while (see the right tip of the crack in Fig. 18 (b)). This provides high signal to noise ratio in the time domain, and is convenient for the post-processing to extract the whole strip of crack. All of these prove the FMRLST has strong flexibility for arbitrary direction of cracks.

It is believed that FMRLST has an overall superiority in combining the scanning coverage and the flexibility for arbitrary cracks, compared to the traditional linear scanning manner. Although it has a blind spot at the rotation center, it can perform a full direction coverage of crack at the rest of the scanned area. The next scan will not only compensate for the blind spot in the previous scan but also increase the inspected area. The traditional linear scanning, however, has to perform twice scans for the same area to finish a single full inspection.

Finally, it should be pointed out that the non-uniformity of the heating will affect the inspection quality. Based on the scanning manner of FMRLST, in the dynamic aspect, it is certain that the heating effect along the rotation radius is different because the linear scan speed of the laser at different distances to the rotation centre is different. In addition, in the static aspect, the line-laser was shaped with 1-dimensional focusing (Powell lens) manner from a Gaussian-distributed circular beam. The energy intensity reduces from the middle to the line tips along the line radius. The non-uniformity will undermine the temperature rise and temperature deviation between the two sides of the crack. Therefore, there is an optimal detection range on the rotation line radius (between the center point to the edge of the scanning circle). This range is determined by the rotation speed, the energy homogeneity of laser-line, and the length of the laser.

It is noticed that the disbond and delamination were also partially detected in the scanning of FMRLST. It has been proved that disbond and delamination can be characterized by Joint Scanning Laser Thermography [26, 27]. It suggests a promising prospect for the FMRLST inspecting disbond when an optimized balance of laser-line dimension, scanning speed, and proper image processing algorithms is furtherly investigated. In future work, it will be investigated to find out the optimal inspection range balancing with the above factors. In addition, more work will focus on the inspection of disbond and delamination mixed with cracks in the impact damage.

VI. Conclusion

In this paper, a Fiber-guided Motorised Rotating Laser Scanning Thermography (FMRLST) system is proposed for the inspection of surface cracks in impact damage in composites. A novel heating manner with rotating laser-line scanning for

thermography testing is designed with a motorized optical head and fiber delivery. The rotating laser-line scanning manner provides superior sensitivity, robustness and applicability to the arbitrary cracks by the unique rotating heat transfer, stimulating the crack edge with a dynamic tangential line pattern. A post-processing method of thermogram based on CT is developed to enhance the contrast and extract multi-direction cracks in impact damage. The thermal sequence processing method is proved to be remarkably appropriate for the rotating heat transfer of FMRLST and achieves crack enhancement, laser-line pattern suppression and noise cancelling simultaneously. The proposed technique is validated by both simulation and experimental testing of impact damage in composites. In experiments, three composite specimens with different levels of impact damage and surface cracks are effectively inspected and extracted. Both surface break cracks, break bumps, and barely invisible cracks are clearly detected with accurate position and crack length. The remarkable applicability and flexibility of FMRLST to arbitrary cracks present its huge potential in on-site thermography inspection, and its design is promising to push the LST towards a miniaturized probe-like inspection system. Further research will focus on the investigation of the parameter optimization (energy, rotating dynamics, laser-line specs.) of the rotating laser, and updating the image processing method to identify multiple defect types.

REFERENCES

[1] P. Irving and C. Soutis, *Polymer composites in the aerospace industry*. Amsterdam: WP, Woodhead Publ./Elsevier, 2015.

[2] T. P. A. Hernandez, and H. Yazdani Nezhad, “Shear driven deformation and damage mechanisms in high-performance carbon fibre-reinforced thermoplastic and toughened thermoset composites subjected to high strain loading,” *Compos. Struct.*, vol. 261, p. 113289, 2021.

[3] S. Yuan, Y. Ren, L. Qiu, and H. Mei, “A multi-response-based wireless impact monitoring network for aircraft composite structures,” *IEEE Trans. Ind. Electron.,* vol. 63, no. 12, pp. 7712–7722, 2016.

[4] R. Talreja and N. Phan, “Assessment of damage tolerance approaches for composite aircraft with focus on barely visible impact damage,” *Compos. Struct.*, vol. 219, pp. 1–7, 2019.

[5] Y. Kong, C. J. Bennett, and C. J. Hyde, “A review of non-destructive testing techniques for the in-situ investigation of fretting fatigue cracks,” *Mater. Des.*, vol. 196, p. 109093, 2020.

[6] H. Liu, S. Liu, Z. Liu and A. S. Milani, "Data-Driven Approaches for Characterization of Delamination Damage in Composite Materials," *IEEE Trans. Ind. Electron.*, vol. 68, no. 3, pp. 2532-2542, 2021.

[7] X. Zhang, Y. He, T. Chady and S. Chen, “CFRP Impact Damage Inspection based on manifold learning using ultrasonic induced thermography,” *IEEE Trans. Ind. Inform.*, vol. 15, no. 5, pp. 2648–2659, 2019.

[8] M. Mirbagheri, O. Rahmani, and Y. Mirbagheri, “Estimation of residual tensile strength of composite laminate after low-velocity impact using visually inspection,” *Eng. Fail. Anal.*, vol. 131, p. 105898, 2022.

[9] Z. Deng *et.al*, “Multi-source effect in magnetizing-based eddy current testing sensor for Surface Crack in ferromagnetic materials,” *Sens. Actuator A Phys.*, vol. 271, pp. 24–36, 2018.

[10] W. Du, H. Shen, and J. Fu, “Automatic defect segmentation in X-ray images based on Deep Learning,” *IEEE Trans. Ind. Electron.*, vol. 68, no. 12, pp. 12912–12920, 2021.

[11] B. Deng, W. Wu, X. Li, Y. He, G. Shen, Y. Tang, K. Zhou, Z. Zhang, and Y. Wang, “Active 3-D thermography based on feature-free registration of thermogram sequence and 3-D shape via a single thermal camera,” *IEEE Trans. Ind. Electron.*, vol. 69, no. 11, pp. 11774–11784, 2022.

[12] Q. Tang, J. Liu, J. Dai, and Z. Yu, “Theoretical and experimental study on thermal barrier coating (TBC) uneven thickness detection using pulsed infrared thermography technology,” *Appl. Therm. Eng.*, vol. 114, pp. 770–775, 2017.

[13] I. Garrido, E. Barreira, R. M.S.F. Almeida, and S. Lagüela, “Introduction of active thermography and automatic defect segmentation in the thermographic inspection of specimens of ceramic tiling for building façades,” *Infrared Phys. Technol.*, vol. 121, p. 104012, 2022.

[14] S. Hwang, Y.-K. An, and H. Sohn, “Continuous-wave line laser thermography for monitoring of rotating wind turbine blades,” *Structural Health Monitoring*, vol. 18, no. 4, pp. 1010–1021, 2018.

[15] T. Aujeszky, G. Korres, and M. Eid, “Measurement-based thermal modeling using laser thermography,” *IEEE Trans. Instrum. Meas.*, vol. 67, no. 6, pp. 1359–1369, 2018.

[16] J. Moran and N. Rajic, “Remote line scan thermography for the rapid inspection of composite impact damage,” *Compos. Struct.*, vol. 208, pp. 442–453, 2019.

[17] J. Qiu, C. Pei, H. Liu, Z. Chen, K. Demachi, "Remote inspection of surface cracks in metallic structures with fiber-guided laser array spots thermography", *NDT E Int*, vol. 92, pp. 213-220, 2017.

[18] J. Wei, F. Wang, J. Liu, Y. Wang, and L. He, “A laser arrays scan thermography (LASST) for the rapid inspection of CFRP composite with Subsurface defects,” *Compos. Struct.*, vol. 226, p. 111201, 2019.

[19] G. Ruipeng, W. Haitao, and Z. Jianyan, “Theoretical and experimental studies on the detection of high-temperature metal surface imperfections susing a scanning laser point source method,” *Insight: Non-Destr. Test. Cond. Monit.*, vol. 59, no. 7, pp. 371–378, 2017.

[20] W. Du, H. Liu, Y. Zhao, A. Sirikham and Y. Zhao, "A Miniaturized Active Thermography System to Inspect Composite Laminates," *IEEE Trans. Ind. Inform.*, vol. 17, no. 5, pp. 3314-3323, May 2021.

[21] M. Mićić, L. Brajović, L. Lazarević, and Z. Popović, “Inspection of RCF rail defects – review of NDT methods,” *Mech. Syst. Signal Process.*, vol. 182, p. 109568, 2023.

[22] H. Liu, W. Du, H. Yazdani Nezhad, A. Starr, and Y. Zhao, “A dissection and enhancement technique for combined damage characterization in composite laminates using laser-line scanning thermography,” *Compos. Struct*., vol. 271, p. 114168, 2021.

[23] F. Lopez, V. Nicolau, C. Ibarra-Castanedo, X. Maldague, "Thermal–numerical model and computational simulation of pulsed thermography inspection of carbon fiber-reinforced composites", *Int. J. Therm. Sci..,* vol. 86, pp. 325-340, 2014.

[24] J. Wang, J. K. Carson, M. F. North, and D. J. Cleland, “A new approach to modelling the effective thermal conductivity of heterogeneous materials,” International Journal of Heat and Mass Transfer, vol. 49, no. 17-18, pp. 3075–3083, 2006.

[25] S. Dubois, R. Péteri, and M. Ménard, “Characterization and recognition of dynamic textures based on the 2D+T Curvelet transform,” *Signal, Image and Video Processing*, vol. 9, no. 4, pp. 819–830, 2013.

[26] Z. He, H. Wang, Y. He, G. Zhang, J. Wang, G. Zou, and T. Chady, “Joint scanning laser thermography defect detection method for carbon fiber reinforced polymer,” IEEE Sensors Journal, vol. 20, no. 1, pp. 328–336, 2020.

[27] Z. He, H. Wang, Y. Li, Z. Zhang, Y. Zhang, H. Bi, and Y. He, “A deconvolutional reconstruction method based on Lucy–Richardson algorithm for Joint Scanning Laser Thermography,” IEEE Transactions on Instrumentation and Measurement, vol. 70, pp. 1–8, 2021.s

Haochen Liu received his Ph.D. degree in mechanical engineering from Xi’an Jiaotong University, Xi’an, China in 2018.
He is currently a research fellow in industrial inspection at Cranfield University, Cranfield, UK. His research interests include InfraRed Thermography NDT, thermal transfer problems, structural health monitor, artificial intelligent inspection, and inverse problem in IR-NDT.

Lawrence Tinsley received an MPhys degree in Physics with Planetary and Space Physics from Aberystwyth University, Wales in 2009, and a Ph.D. from Cranfield University, UK, in 2020.
He is currently working as a research fellow in industrial inspections, at Cranfield University, where his research includes non-destructive testing, thermography, eddy current testing, and development of digital twins.

Kailun Deng received his M.Sc. degree in engineering and management of manufacturing systems in 2018 from Cranfield University, Cranfield, U.K.
He is currently working toward the Ph.D. degree, focusing on developing an intelligent pulsed thermographic inspection system powered by artificial intelligence (AI) and augmented reality (AR) technologies.

Yizhong Wang, PhD student in the Cranfield University, focuses on Non-destructive testing (NDT), sensor information fusion, computer vision and machine learning. He studied Industrial Engineering at University of Pittsburgh and Sichuan University for undergraduate, and Aerospace Manufacturing at Cranfield University for master.

Andrew Starr received his Ph.D. degree from the University of Manchester, Manchester, UK in 1993. He is currently a Professor of Maintenance Systems at Cranfield University, Cranfield, UK. His research interests include machine and structural damage detection, diagnostics and prognostics, autonomous inspection, "big data" for system monitoring and control, applications in railway infrastructure and vehicles.

Zhenmao Chen received his Ph.D. degree from The University of Tokyo, Tokyo, Japan, in 1998.
He is currently a Professor in Xi'an Jiaotong University, Xi'an, China. His research interests include ElectroMagneto-Thermal-Structural Coupling Mechanics, electromagnetic NDT and applications to nuclear power plants, inverse sproblem and applications to NDT&E, Development of advanced NDT techniques;

Yifan Zhao received the Ph.D. degree in Automatic Control and System Engineering from the University of Sheffield, Sheffield, UK, in 2007.
He is currently a Reader in Data Science at Cranfield University, Cranfield, UK. His research interests include machine learning, computer vision, signal processing, non-destructive testing, active thermography, and nonlinear system identification.

A fiber-guided motorized rotation laser scanning thermography technique for impact damage crack inspection in composites

Liu, Haochen

2023-04-11

Liu H, Tinsley L, Deng K, et al., (2024) A fiber-guided motorized rotation laser scanning thermography technique for impact damage crack inspection in composites. IEEE Transactions on Industrial Electronics, Volume 71, Issue 3, March 2024, pp. 3163-3172

https://doi.org/10.1109/TIE.2023.3265034